



Intra-urban spatial variability of surface ozone and carbon dioxide in Riverside, CA: viability and validation of low-cost sensors

5 Kira Sadighi¹, Evan Coffey¹, Andrea Polidori², Brandon Feenstra², Qin Lv³, Daven K. Henze¹, Michael Hannigan¹

¹University of Colorado Boulder, Department of Mechanical Engineering, 427 UCB, 1111 Engineering Drive, Boulder, CO 80309, USA

²South Coast Air Quality Management District, Air Quality Sensor Performance Evaluation Center, 21865 Copley Drive, Diamond Bar, CA 91765-4178, USA

³University of Colorado Boulder Department of Computer Science, 430 UCB, 1111 Engineering Drive, Boulder, CO 80309, USA

Correspondence to: Kira Sadighi (Kira.Sadighi@colorado.edu)

Abstract. Sensor networks are being more widely used to characterize and understand compounds in the atmosphere such as ozone and carbon dioxide. This study employs a measurement tool, called the U-Pod, constructed at the University of Colorado Boulder, to investigate spatial and temporal variability of O₃ and CO₂ in a 314 km² area of Riverside County near Los Angeles, California. This tool provides low-cost sensors to collect ambient data at non-permanent locations. The U-Pods were calibrated using a pre-deployment field calibration technique; all the U-Pods were collocated with regulatory monitors. After collocation, the U-Pods were deployed in the area mentioned. A subset of pods was deployed at two local regulatory air quality monitoring stations providing validation for the collocation calibration method. Field validation of sensor O₃ and CO₂ measurements to 10 minute resolution reference observations resulted in R-squared and root mean squared errors (RMSE) of 0.95 – 0.97 and 4.4 – 7.2 ppbv for O₃ and 0.79 and 15 ppmv CO₂, respectively. Using the deployment data, ozone and carbon dioxide concentrations were observed to vary on this small spatial scale. In the analysis based on hourly binned data, the median R-squared values between all possible U-Pod pairs varied from 0.52 to 0.86 for ozone during the deployment. The medians of absolute differences were calculated between all possible pod pairs, 21 pairs total. The median values of those median absolute differences for each hour of the day varied between 2.2 and 9.3 ppb for the ozone deployment. For carbon dioxide, distributions of all measurements vary from 413 – 425 ppm during the calibration (collocation) and 406 – 472 during the deployment. Since 15 median differences between U-Pod concentrations during deployment are larger than the respective root mean square error values for ozone and carbon dioxide, we can conclude that there is spatial variability in these pollutants across the study area. This is important because it means that citizens may be exposed to more ozone than they would assume based on current 20 regulatory monitoring.

25



1 Introduction

Tropospheric ozone formation and destruction is a complex chemical process involving a series of interdependent chemical reactions of volatile organic compounds (VOCs) and nitrogen oxides (NO_x) in the presence of ultraviolet (UV) radiation (Jacob, 2000). The reactants are produced and consumed both naturally and through anthropogenic activities, as well as through atmospheric chemical reactions. In urban areas, the sources of these emissions and their impact on ozone formation vary in time and space. For example, trucks and cars, acting as mobile sources of primarily NO_x and VOCs, respectively, contribute to the formation and/or destruction of ozone depending on mixing ratios of each and the presence of UV radiation. Due to the health implications of increased ozone exposures, local, regional and national regulatory bodies have the obligation to measure, report and mitigate ambient ozone levels according to the National Ambient Air Quality Standards (NAAQS) (EPA 2013).

10

The equipment employed at air quality monitoring stations (AQMS) is expensive and requires substantial resources to maintain. As such, increasing the spatial resolution of the AQMS network is not readily feasible. Thus, one benefit of low-cost, portable sensing technology is the ability to collect data at more locations, increasing spatial resolution of existing AQMS. Detecting pollutant variability between the regulatory AQMS supports the idea that more detailed information can be obtained by increased monitoring between the existing stations.

15

Regulatory monitoring for compliance with the ozone NAAQS is undertaken as dictated by the Code of Federal Regulations, which states, “The goal in locating monitors is to correctly match the spatial scale represented by the sample of monitored air with the spatial scale most appropriate for the monitoring site type, air pollutant to be measured, and the monitoring objective.” (EPA, 2006). Ozone monitoring site types include: highest concentration, population oriented, source impact, general/background and regional transport, and welfare-related impacts. Siting involves choosing a monitoring objective, selecting a location that best achieves those goals, and determining a spatial scale that fits the monitoring objective.

20

Carbon dioxide measurements are a special concern to organizations such as the California Air Resources Board (CARB) and others for providing information on combustion emissions as well as greenhouse gas concentrations (Verhulst et al., 2016). One of the most difficult aspects of measuring CO₂ in urban areas is the collocated nature of anthropogenic and biogenic sources and sinks, and difficulty in isolating these components (Verhulst et al., 2016, Hutyra et al., 2014, Kort et al., 2013). However, accurate measurements of carbon dioxide in cities will become increasingly important for carbon cycle and climate change science (Hutyra et al., 2014). This will be especially important in a Megacity like Los Angeles, where CO₂ is highly variable across the region (Verhulst et al., 2016). Kort and coworkers suggest that networks of carbon dioxide measurements with high spatial and temporal variability are necessary to properly study greenhouse gas fluxes in the Los Angeles area (Kort et al., 2013). Hutyra and coworkers also stress the importance of complete datasets that also report the level of uncertainty (Hutyra et al., 2014). Low-cost sensor networks could help to tackle some of these challenges. The analysis of carbon dioxide

25

30



data in this study seeks to explore the extent of spatial and temporal variability, while framing those findings in measurement uncertainty.

The minimum number of sites required in Riverside-San Bernardino counties is three (given the population is between four
5 and ten million). As of 2013, there were 20 active sites measuring ozone in Riverside and San Bernardino counties (California
Air Resources Board, 2013). For our CyberSEES project (NSF Award ID: 1442971), the measured variability between AQMS
will provide validation for atmospheric model downscaling to the 10s of kilometer scale – smaller spacing than current EPA
monitoring networks. The current spacing is not sufficient to capture high spatial resolution concentrations (Bart et al., 2014;
Moltchanov et al., 2015). Additionally, this variability could potentially be used to inform exposure assessment for health
10 studies as well as improve our understanding of pollutant sources and fate (Simon et al., 2016; Lin et al., 2015; Blanchard et
al., 2014).

Networks of air quality sensors have been deployed in various settings. Moltchanov and coworkers measured O₃, NO₂ and
VOCs in Haifa, Israel in the summer of 2013 to test the viability of sensor networks measuring small scale (100s of meters)
15 intra-urban pollution (Moltchanov et al., 2015). They found variations in microenvironmental pollutant concentrations, but
lacked robust in-field sensor validation. Two of their sites (A and B) had correlations between 0.82 and 0.94 with each other,
but correlations between A or B and C were much lower, between 0.04 and 0.72. Mead and coworkers established static and
mobile air quality sensor networks in Cambridge, UK measuring CO, NO and NO₂ with electrochemical sensors while
performing similar campaigns in Spain and Nigeria (Mead et al., 2013). In 2013, Williams and coworkers quantified a tungstic
20 oxide ozone sensor in the lab while addressing some of the main drawbacks associated with Metal oxide (MO_x) ozone sensors
(i.e. drift/long term stability, material degradation and sensitivity fluctuations) (Williams et al., 2013). Researchers also
deployed these gas semiconductor sensors in British Columbia over roughly 10,000 km² for three months finding low errors
(3 +/- 2 ppb) between hourly averaged sensor and reference instruments while documenting the challenges of using, in this
instance, wireless sensor networks (Bart et al, 2014). Lin and coworkers demonstrated high correlations (0.91) between
25 tungsten oxide semiconductor ozone sensors and hourly averaged Federal Reference Method (FRM) chemiluminescence gas
analyzer measurements in Edinburgh, UK with similar magnitudes (Lin et al., 2015).

Here we specifically seek to answer the question, are these sensors able to detect significant differences on scales that are
smaller than current EPA reference stations, given their quantification uncertainty? This study is unique in that the Inland
30 Empire region of the greater Los Angeles area frequently experiences very high levels of ozone. The combination of sunlight
and high VOCs is ideal for the formation of ozone. The Pacific inversion layer over southern California and mountains that
form a natural basin act together to keep pollutants from dissipating (Littman and Magill, 1953). As such, Riverside, CA is an
ideal test bed to answer our question.



2 Methods

This field study was conducted within a 314 km² area of Northwestern Riverside County, California, a region frequently designated as “nonattainment” for failing to meet requirements for ozone and particulate matter designated by the EPA (EPA, 2016). Thirteen low-cost monitors were deployed within a 10 km radius in Riverside in the summer of 2015 (Fig. 1). These monitors were sited in the cities of Riverside and Jurupa Valley with the aid of the South Coast Air Quality Management District (SCAQMD). Sites were chosen based on availability and power access. Ten locations were identified (Fig. 1) representing a variety of site conditions ranging from university campuses and residential neighborhoods to commercial and industrial zones. Within this area, there are two regulatory AQMS that measure O₃: Rubidoux and Mira Loma. The transportation authority in California, Caltrans, records traffic volume information for many large highways. Annual average daily traffic (AADT) is recorded at many road intersections. On two major roads in the study area in this region, specifically Hwy 91 and Hwy 60, the averaging of all the milepost traffic count data between junctions shows AADTs of 180,500 and 220,500, respectively (“2015 Traffic Volumes”, 2017). Van Buren Avenue does not have AADT data. However, it has two lanes each way, while the other highways have more than four. In general, there are a high number of vehicles traveling around and through this study area daily; these vehicles likely represent the dominant sources of CO₂, NO_x, and VOCs.

15

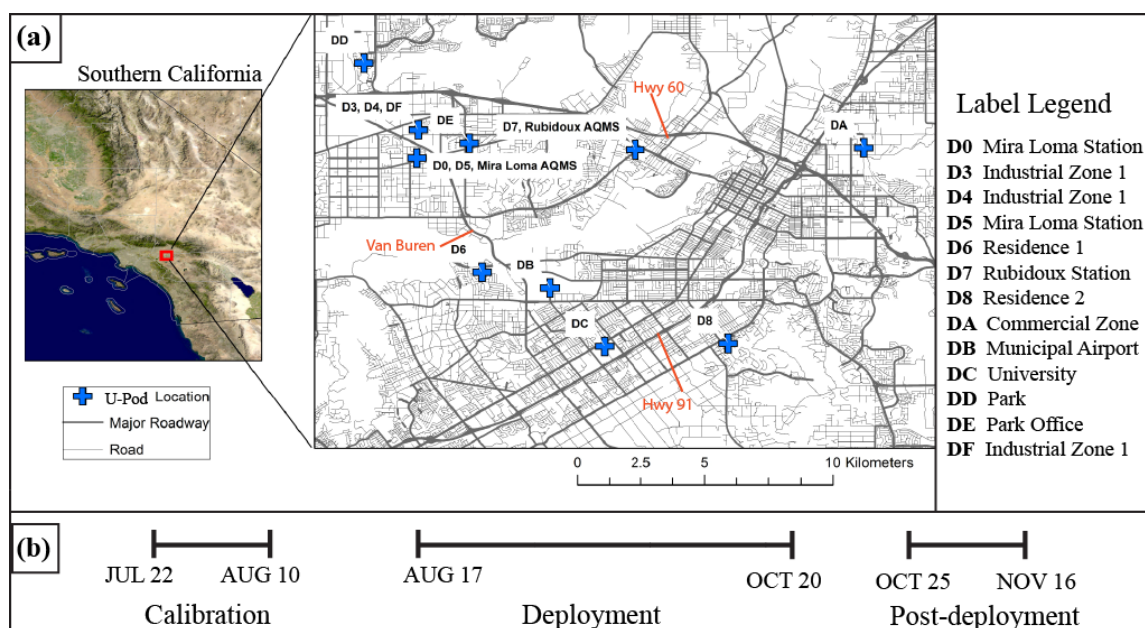


Figure 1. (a) A Map of the deployment area. The crosses indicate U-Pod locations, with the AQMS labelled by name and (b) a timeline of project phases, from calibration, to deployment and post-deployment



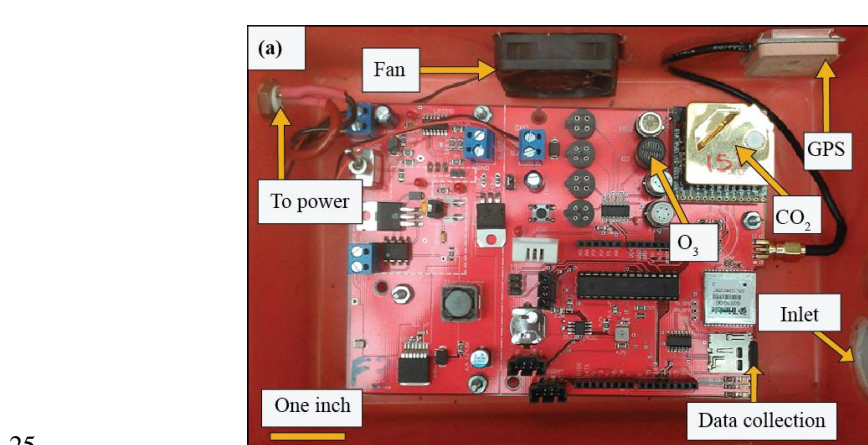
2.1 Low-Cost Monitor

Measurements were taken using the University of Colorado U-Pod air quality monitoring platform (mobilesensingtechnology.com) described in previous work (Piedrahita et al. 2011). Briefly, the U-Pod consists of an Arduino data acquisition system and a suite of environmental sensors enclosed in a small, ventilated, portable case (Fig. 2). Specifically, O₃ is measured using a metal oxide sensor, MO_x, (MiCS 2611, SGX Tech. formerly e2v ~ \$11), CO₂ is measured with a low-cost non-dispersive infrared (NDIR) sensor (S200/300, ELT Corp. ~\$50). Enclosure air temperature and relative humidity were also measured. U-Pod locations were verified using an on-board GPS chip and all data were saved to a micro SD card. Logged data were collected into minute medians to match the highest temporal resolution of nearby regulatory air quality stations. Duplicate O₃ sensors were included in most U-Pods to investigate innate sensor variability and model performance.

10

MO_x sensors operate through reduction/oxidation processes at the gas-semiconductor surface resulting in changes in electrical resistance (Korotcenkov et al. 2007). This change in resistance is in part a function of the concentration of the target gas (i.e., ozone) in the surrounding air, as well as temperature and humidity. A detailed summary of MO_x gas sensors by Korotcenkov and coworkers documents potential issues of using sensors in long term ambient monitoring campaigns (Korotcenkov et al., 2007). A variety of environmental factors such as long term exposure to water causing hydration of the oxide surface layer leads to drift in the sensing chemistry, as well as cross sensitivity to other oxidizing species like NO_x. However, due to the low-cost nature of such sensor technology, the use of MO_x gas sensors in ambient monitoring is being widely pursued. NDIR sensor technology uses optical absorption in the IR band to measure CO₂ gas concentration, among other compounds. Most commercialized NDIR sensors commonly contain low-cost mini-filament bulbs (as opposed to LEDs), as do the ELT Sensor Corp. S-300 and S-300A models of the CO₂ sensors used in this study (Bogue, 2013). These sensors operate between -10 and 60 degrees Celsius. They can perform in relative humidity levels between 0 and 95 percent. More information about these specific carbon dioxide sensors is available at http://www.eltsensor.co.kr/2016/products/oem_modules/S-300.html.

15



25



Figure 2. (a) Demonstration of the U-Pod layout, including sensor locations and other features. (b) A photo of the field calibration collocation at Rubidoux AQMS.

2.2 Field Calibration

Sensors were calibrated using a field calibration technique, commonly employed with low-cost sensor networks, which involves collocating sensors with a reference grade monitor for an extended period of time prior to and directly following a field deployment (Piedrahita et al, 2011). The concept of field calibration is straightforward; develop relationships between the reference measurement and pollutant sensor signal using combinations of concurrently collected environmental data. All U-Pods were calibrated at the SCAQMD Rubidoux AQMS (elev. 248m above sea level) for three weeks, July 22 – Aug 10, prior to the field deployment. The Rubidoux station sampling scale is classified as “urban” for ozone and is located 119 m from Hwy. 60 (SCAQMD, 2015). Reference ozone is measured using a designated Federal Equivalent Method (FEM) Thermo 49i dual cell UV photometric monitor. CO₂ was measured using an infrared LI-840a gas analyzer (LI-COR) which was lab-calibrated at the University of Colorado, using three certified gas standards (0, 287 and 1990 ppm) prior to the campaign. Numerous field calibration relationships were developed using a suite of custom MATLAB codes. This process involves performing linear and nonlinear regressions using sensor signal, measured U-Pod enclosure temperature, absolute humidity and time (to account for sensor drift) against the reference gas concentrations. MO_x sensor signals are the ratio of instantaneous resistance to a reference resistance defined during the field calibration. For the NDIR carbon dioxide sensors, the signal is an analog output. To evaluate the resulting regression fit, we used coefficient of determination (R²), root mean square error (RMSE) and explored residuals with relation to each input variable, specifically looking for normal distributions. Through this process, we discovered that an interaction term between temperature and ozone concentration improved the model fit at higher mixing ratios leading to overall higher correlations, lower error, and improved residual distributions (see Table 1). The best performing model for ozone during calibration incorporates temperature, absolute humidity, and time (Eq. 1).

$$S = p_1 + Cp_6(T + p_2) + TAp_3p_4 + (t - t_o)p_5 \quad (1)$$

Where S is the sensor signal in R/R_o, where R is the sensor resistance and R_o is a chosen normalizing resistance value. C is the pollutant concentration in ppb or ppm, T is the temperature in Kelvin, A is absolute humidity in mole fraction, and the p variables are coefficients. In this model, a global absolute humidity term was employed; this absolute humidity was calculated using Rubidoux reference station temperature and relative humidity, and a constant pressure.

For CO₂ data, the best model incorporates the same variables as Eq. (1), but in a slightly different combination (Eq. 2).

$$S = p_1 + Cp_2 + Tp_3 + Ap_4 + (t - t_o)p_5 \quad (2)$$

2.3 Field Validation of Model Performance

A nearly three month long validation dataset was collected to quantify the performance of the generated calibrations in the field. Previous air quality sensor campaigns have either had mixed results when performing validation in the field or no validation was included. Moreover, no study, to our knowledge, has validated ozone and carbon dioxide sensor measurements



to reference grade monitors at one-minute resolution. Two validation approaches were investigated here. First, we compared sensor measurements to reference grade observations in the *same* location as was used for the field calibration. Second, we compared sensor measurements to reference grade observations in a location that was different from the field calibration site. The second approach can be used to address error associated with site specific confounders, such as NO_x or transient temperature effects present outside the calibration microenvironmental space. U-Pod D7 was validated using the first approach, as it remained at Rubidoux AQMS for the duration of the deployment. U-Pods D0 and D5 were moved from Rubidoux AQMS, after the calibration, to Mira Loma AQMS and validated using the second approach. The outcome of the field validation methods is presented in the results.

3 Results

3.1 Field Calibration Results

Results of the field calibration process are provided in Table 1 and sample models are shown in Fig. S1 and S2 (for ozone and carbon dioxide, respectively). For O₃, the best model statistics were observed for the four term (4T) linear equation. R² values and errors (RMSE) range from 0.97 – 0.99 and 1.8 – 3.9 ppbv, respectively. There were three other regression equations tested that fit less well; those fit statistics are presented in Table S1.

CO₂ calibrations were less precise, with R² and RMSE ranging from 0.44 – 0.92 and 9.0 – 77 ppmv, respectively (Table S1). Inherent CO₂ sensor auto-calibration likely caused these variations in calibration performance because of automated baseline and sensitivity shifts over time, as well as increased noise in this sensor compared to ozone.

Table 1: Field calibration results of the Linear 4T model for ozone sensors showing R² and RMSE with the reference monitor data. Two O₃ entries means there are two different sensors in the same U-Pod.

U-Pod ID	D0	D3	D4	D5	D6	D7	D8	DA	DB	DC	DD	DE	DF
R ² , RMSE	0.98, 3.1	0.98, 3.0	0.98, 2.6	0.99, 2.7	0.98, 3.5	0.98, 2.8	0.98, 3.0	0.97, 3.9	0.98, 2.8	0.99, 2.6	0.99, 1.8	0.97, 3.4	0.98, 3.1
	0.98, 3.2	0.98, 3.0	0.98, 2.7	0.98, 3.0	0.99, 2.4	0.98, 3.0		0.97, 3.9		0.98, 2.7	0.99, 1.8	0.98, 2.9	0.98, 3.0

3.2 Deployment Data Filtering and Processing

Some temperature and humidity values were experienced by the U-Pods during the deployment that were not experienced during the calibration time period. This means that the environmental parameter space sampled during the calibration time did



not cover the parameter space experienced during the rest of the summer. Including those data points in subsequent analysis would be a form of extrapolation that can either be assessed or avoided. As such, the U-Pod deployment data were filtered for environmental variables, an example of which is shown in Fig. 3. The global absolute humidity in Fig. 3a is the same for all U-Pods. Normally, the absolute humidity would be calculated for each U-Pod using its individual recorded temperature, relative humidity, and pressure. However, during the deployment, the relative humidity sensors failed in several U-Pods. Because of this, temperature and relative humidity data from Rubidoux AQMS, along with a constant pressure value were used to calculate the global absolute humidity for the Riverside area for each minute. During calibration, the same values of absolute humidity were used for each U-Pod, but temperatures were pod specific.

10

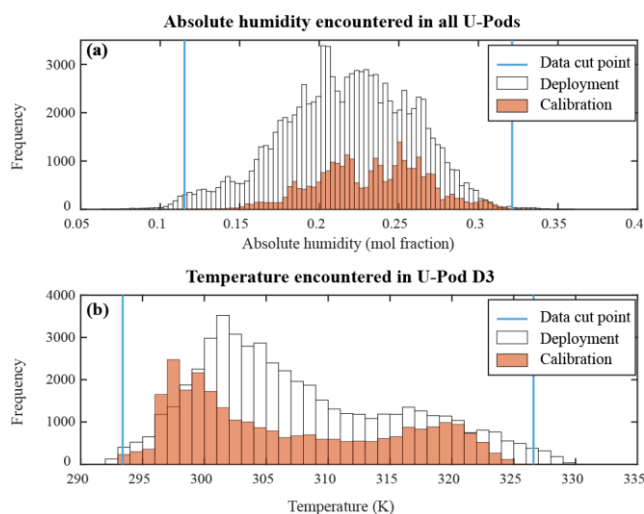


Figure 3. This is an example for one U-Pod (D3) showing lower absolute humidity (a) and higher temperatures (b) occurred during the deployment than during the calibration. The data cut point shows where minimum and maximum values of the variables included in the data are.

15

In addition, deployment data were filtered for maximum and minimum values of O_3 ; again, we wanted to minimize model extrapolation. The difference between the maxima of the Rubidoux and the Mira Loma air quality monitoring stations was 2 ppb for the deployment period, or 7 % of the highest maximum value recorded by either station. For O_3 , values that resulted in concentrations that were over 7% of the highest maximum value (148 ppb) were removed. No minimum filtering was needed for O_3 . For CO_2 , there was no maximum or minimum filtering.

20

Lastly, data were filtered using consecutive differences. Data were omitted when they fell more than eight standard deviations away from the mean consecutive difference in values. This is a standardized way to cut out spikes in data caused by power



control issues. The results of the deployment data filtering are shown in Table S2. Most U-Pods have two ozone sensors, and one CO₂ sensor.

Subsequently, U-Pod DD was omitted from this analysis due to a lack of data. This pod lost almost 46% of its data after the filtering process and collected less data to begin with than the others. U-Pods D4, D5, D6, D8 and DF required a modification be made to the CO₂ sensor, with the goal of disabling the auto-calibration setting. For the ELT-300 model, this auto-calibration happens during “dimmed” light settings for indoor monitoring, creating challenges for ambient monitoring. This electrical modification to the U-Pod system appeared to have shifted ozone baseline signal values resulting in biased values for D5. In a conservative effort, all U-Pods that were modified as described above were removed from the subsequent ozone analysis. Since some U-Pods were at the same location, the removal of these U-Pods from analysis resulted in the loss of two sites from the study. The other sites had a least one U-Pod remaining.

3.3 Field Calibration Validation Results

All regression models shown in Table S1 were applied to the filtered validation datasets. The best performing model was selected based on R², RMSE and residual distributions. Ozone concentrations were best modelled using the linear4T model, similar to what was observed for the calibration. Carbon dioxide concentrations were best modelled using a linear relationship with sensor signal, absolute humidity and temperature, dubbed Linear3 (Eq. 2). Results from both field validation methods are presented in Figs. S3, S4 and S5, and summary statistics are shown in Table 2.

We thought that the first validation method (U-Pod in the same location, D7) would have better validation statistics than U-Pods validated using the second method (U-Pod relocated to a different location, D0 and D5). However, in viewing the statistics, this is not the case as both O₃ sensors in U-Pod D0 show better or similar performance to the Mira Loma station reference data than the two sensors in U-Pod D7 compared to the Rubidoux station reference concentrations.

SCAQMD performed nightly precision checks (PC) of ozone between 90 – 100 ppbv. When PC measurements deviated more than 5% from expected values, subsequent data would be flagged and a work order would be generated for service or calibration. This corresponds to a concentration of about 5 ppb. Values that are less than around 5 ppb different than expected, would not be flagged. This serves as a reference point for the quality of the reference ozone measurements. During the validation, our O₃ sensors had a measurement error (RMSE), for minute median data, which ranged from 4.45 to 7.16 ppb. For each sensor, the median of the residuals ranged from 0.86 to 7.15 ppb, while mean of the residuals ranged from 0.7 to 6.4 ppb. Both median and mean of the residuals were calculated to assess bias. As discussed earlier, U-Pod D5 experienced an electrical issue during the calibration period which resulted in a clear bias throughout the validation dataset. This particular electrical issue points to the challenges of using such sensor platforms in an ambient monitoring context, a topic widely discussed in the air sensor community (Kumar et al. 2015). Bias for the other U-Pods was relatively small and on the order of 1 – 2 ppbv.



For CO₂, the RMSE was 15.0 ppmv. The sensor was under-predicting at higher concentrations and higher absolute humidity, and slightly over predicting at elevated temperatures and as the deployment progressed (Fig. S6).

- 5 In order to gain a better understanding of the dependency of model performance on the selection of the validation data, we repeated this assessment with 200 iterations of 10% randomly sampled minute level deployment data. The values of the statistics could be affected by which time period the validation data is selected from. For example, choosing 10% of consecutive data from the first few days could give misleading statistics. The resulting distributions for the performance metrics are shown in Table 2. The +/- indicates the range of values observed during all the iterations. Tight distributions show little dependence
- 10 on the data selected.

Table 2. Validation sensitivity results showing mean residuals, median residuals, R² and RMSE of sensor measurements against Rubidoux or Mira Loma AQMS observations for O₃ (ppbv) and CO₂ (ppmv). Two-hundred iterations of 10% of randomly chosen data was used for validation statistics. The residuals are U-Pod data – reference monitor data.

U-Pod ID/species	mean residual	median residual	mean R ²	mean RMSE
D7 O ₃ Sensor 1	2.4 +/- 0.1	1.2 +/- 0.1	0.965 +/- 0.001	5.6 +/- 0.1
D7 O ₃ Sensor 2	2.8 +/- 0.1	1.5 +/- 0.1	0.963 +/- 0.001	5.9 +/- 0.1
D0 O ₃ Sensor 1	0.7 +/- 0.1	0.8 +/- 0.1	0.974 +/- 0.001	4.4 +/- 0.1
D0 O ₃ Sensor 2	1.1 +/- 0.1	1.0 +/- 0.1	0.971 +/- 0.001	4.9 +/- 0.1
D5 O ₃ Sensor 1	5.5 +/- 0.1	5.1 +/- 0.1	0.971 +/- 0.001	5.0 +/- 0.1
D5 O ₃ Sensor 2	6.4 +/- 0.1	3.9 +/- 0.1	0.953 +/- 0.001	7.2 +/- 0.1
D7 CO ₂	3.0 +/- 0.3	3.0 +/- 0.3	0.789 +/- 0.007	15 +/- 0.2



3.4 Deployment Data

The aim of our data analysis is to present spatial differences of U-Pod measurements that include measurement uncertainty, and thus allow us to understand the ability of the sensors to detect variability. To examine this spatial variability, we computed the R^2 values and median absolute differences for all possible U-Pod pairs. Unless otherwise stated, median minute time resolution data recorded during the approximately 11 week deployment were used in the following analysis. The calibration model obtained during collocation was applied to all data. Applying the linear model to the U-Pod data collected during the collocation yields the best possible accuracy of the U-Pod sensors, as the model is being applied to the data from which it was derived. As such, comparisons of collocation data and deployment data are useful as the “variability” observed in the collocation data approximates that measurement uncertainty, and as such comparing that “variability” to the variability observed when the U-Pods are deployed allow us to investigate our ability to observe actual spatial and temporal differences.

3.4.1 Ozone

The U-Pods sampled for approximately 2900 hours total, 58% of which consisted of the deployment period data. The medians of ozone value distributions by U-Pod during the calibration range from 29 to 30 ppb. The 5% percentile values range from 2 – 5 ppb and the 95th percentiles were 70 – 83 ppb. During deployment, the median ozone distribution values were between 14 and 31 ppb. The 5th percentile range for deployment was 0 – 6 ppb while the 95th percentile was 67 – 99 ppb.

Ozone concentrations experience a diurnal cycle. This cycle usually incorporates low ozone at night and during the early morning, and a peak in concentration sometime during the day. The precursors to forming ozone: sunlight, VOCs and NO_x also have daily cycles, that in turn affect the ozone cycle profile (Gao, 2007). Figure 4 shows the diurnal cycle for ozone based on concentrations collected during this study.



Concentration distributions of ozone during the deployment

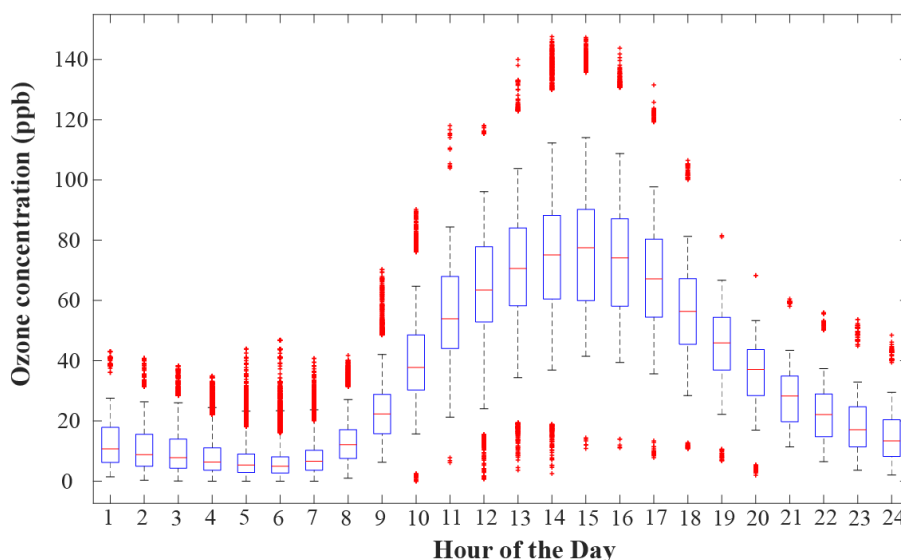


Figure 4. The diurnal cycle of ozone during the deployment. Distributions are concentrations from all U-Pods during each hour. Whiskers indicate the 5th and 95th percentile, with + marks falling outside of this range. The box boundaries span the 25th to 75th percentiles.

5

Figure 4 gives some context temporal variability in ozone concentrations in this study looks like. There are some trends in ozone across the Southern California that we would expect to see. Ozone generally is inhibited in the early morning, followed by midday growth and a peak in concentration. For the remaining hours, ozone concentrations generally decrease, although emissions from the previous day may have effects on concentrations during the next (Gao and Niemeier, 2007). For this study, ozone is lowest from midnight to 6:00. Then the accumulation period takes place between 6:00 and 14:00. Peak concentrations occur between 14:00 and 16:00, and for the remaining hours, concentrations decrease again.

10

We examined the R^2 values for all possible U-Pod pairs for each hour of the day to understand spatial variability. The larger the spread and magnitude of the R^2 values, the more spatial variability was likely present in that hour across the study region. Figure 5 shows this correlation information between U-Pods for each hour of the day for ozone. For this plot, all U-Pod data were binned by hour. Then within those bins, correlations were performed for every possible U-Pod pair. As such, each boxplot consists of 21 points.

15

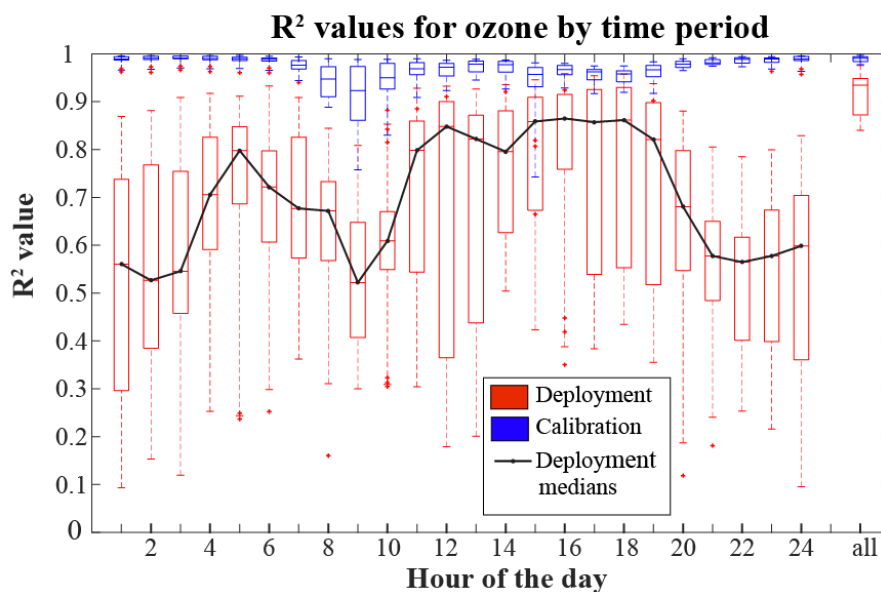


Figure 5. Each boxplot is a collection of the R^2 values between every pair of U-Pods for each hour of the day. There are 21 points in each boxplot. Medians of distributions are marked by horizontal lines. Whiskers indicate the 5th and 95th percentile, with + marks falling outside of this range. The box boundaries span the 25th to 75th percentiles. U-Pod

5

The U-Pods are more correlated to each other during calibration than deployment. The R^2 values between collocated pods are very high, with their medians varying from 0.92 – 0.99 ppb. Conversely, spatially distributed pods were less correlated with each other, leading to R^2 distribution medians between 0.52 and 0.86. The “all” category in Fig. 5 represents the R^2 values between U-Pods, without binning by hour. The medians for the calibration and deployment in this column respectively are

10 0.99 and 0.93 ppb. It is only when binning by hour that greater differences are seen. U-Pods are most different from each other during the hours from 21:00 to 3:00, and at 9:00. U-Pods are most similar around 5:00 and between 11:00 and 19:00. Relationships in R^2 values between pods are changing most quickly through time between 3:00 and 11:00, and again between 19:00 and 21:00.

15 Absolute O_3 concentration differences between pairs of U-Pod were also examined to understand temporal and spatial variability. Figure 6 shows distributions of median absolute differences. All the minute median U-Pod data was time-matched and binned by the hour. Hourly datasets were paired to include every possible U-Pod pair. Within the time matched pairs, the median absolute difference between the two U-Pods were calculated. The distributions in Fig. 6 consist of those 21 points for each hour. The median values of these boxplots increase during the middle of the day, with two major increases observed at

20 hours 10:00 and 15:00, and were lower during the night and early morning.

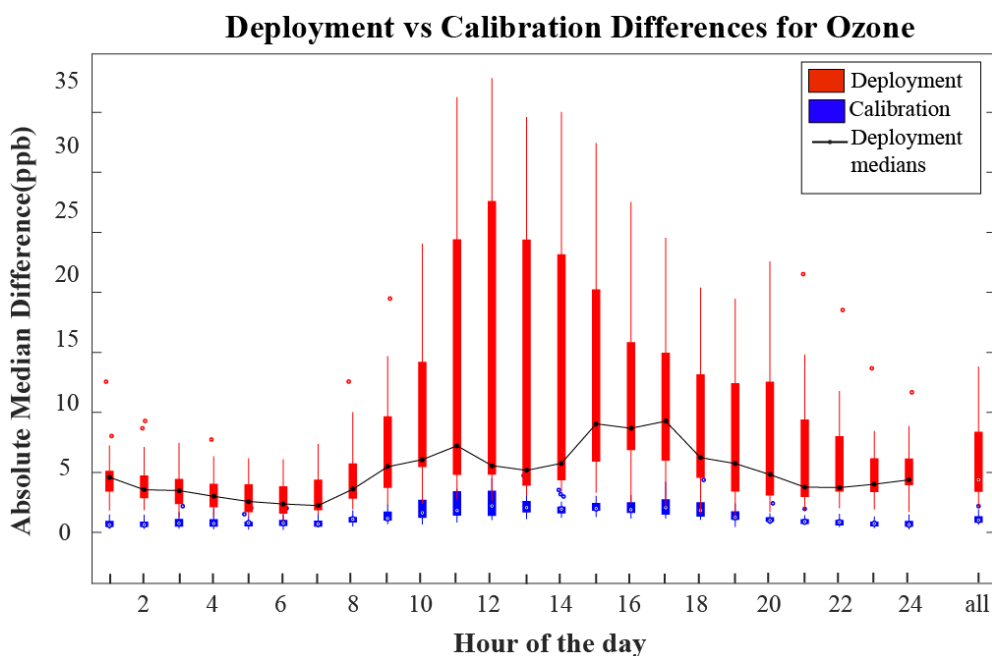


Figure 6. Distributions of medians of absolute differences between all pairs of pods for each hour of the day. Whiskers show 95% intervals. The black line connects the medians of the deployment.

5 We expected that times of day where the spatial variability was the lowest (R^2 highest) the smallest values of absolute differences would be observed. In other words, the deployment medians in Figs. 4 and 5 were expected to have an inverse relationship. There is an increase in R^2 while there is a decrease in absolute median differences around 4:00 to 5:00. There is also an increase in the differences that correspond to increasing R^2 with a peak around 9:00. The absolute median differences reach their minimums and maximums later than the R^2 values reach theirs by a few hours. However, the second jump in median

10 absolute differences between 15:00 and 17:00 was not reflected in reduced R^2 values during those same hours. From 6:00 to 10:00, the slope for the deployment medians in Fig. 6 is steep, indicating that pod differences were increasing quickly across the region, and over that same time period the spatial correlation was lower. The slope between 13:00 and 15:00 looks similar, but the R^2 values were roughly stable and relatively high. In other words, we observed spatial concentration differences and low correlation during the morning commute times, but in the afternoon when we observed the maximum concentration

15 differences, we also observed relatively high spatial correlation. Absolute differences are growing during the morning period and into the afternoon, but since the whole area is experiencing accumulation, there is an increase in correlation as well. Furthermore, although Figure 4 shows high concentrations during the day, Figure A1 demonstrates that percent differences at these times are lower.



Towards the end of daylight hours, between 16:00 and 20:00, the medians of absolute concentration differences have a decreasing trend in time of day, which should be indicating that the pods are becoming more similar because their differences are smaller. However, in the same hours and later, the R^2 values between all U-Pods decrease over time and remain low during the night, indicated that U-Pods are more different from each other than during the afternoon. Some studies have assumed negligible ozone precursor spatial differences in the first hours of the day and therefore spatial ozone homogeneity during the early morning hours (Moltchanov et al., 2005; Jiao et al., 2016). Figure 6 shows that the range of spatial absolute differences in O_3 is smallest at night. However, Fig. 5 suggests that spatial correlation at night is relatively low, causing concern for assumptions about the homogeneity of ozone concentrations at night for this location, although it may apply to others.

To further understand the factors impacting the observed spatial variability, we examined U-Pods individually in more detail. We undertook this investigation by comparing each U-Pod to a common reference U-Pod, to illuminate differences between locations in a normalized way. If no spatial variability were observed, then comparing two U-Pods' ozone measurements would show a 1:1 relationship. To explore this analysis, U-Pod D7 was used for normalization. U-Pod D7 was never moved from Rubidoux station throughout the project and has a validation set. A U-Pod was used as the normalization instead of an AQMS reference monitor in order to compare two similar types of measurement. Differences between calibration period trends and deployment trends were analyzed (Fig. 7) as well as hourly trends by pod (Figs. 7 and 8).

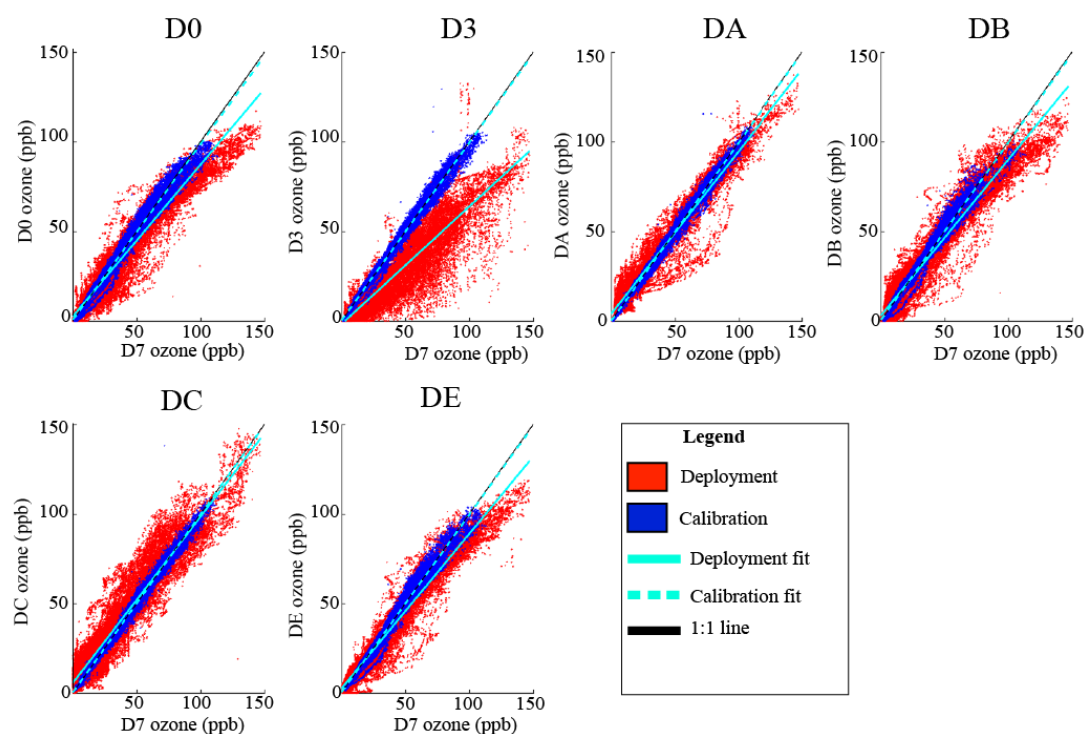




Figure 7. U-Pod D7 ozone concentrations are plotted on the x-axis and other U-Pod ozone concentrations recorded at the same times are on the y-axis. The sets are color coded according to time period their data were taken, and each color is fit with a linear line.

5 In Fig. 7, the calibration data points, representing collocated O_3 measurements, are consistently more densely grouped than the red data points which show the spatial deployment data. This further demonstrates that individual U-Pods were observing spatial differences in O_3 . The deployment O_3 concentrations for U-Pod D3 features a trend that differs significantly from its calibration set. Also, D0, DA, DB, and DE have interesting deviations of O_3 concentrations away from the central cloud of deployment points, in the form of curved areas away from the center line. The deployment trend line slopes are lower than the
10 calibration slopes. As such, U-Pod D7 at the Rubidoux site typically measured higher O_3 than the other U-Pods that were spatially deployed.

Examining the data in this way allows for detailed comparison of U-Pods at different sites. For example, sites D0, D3 and DE were not more than 1.8 km away from each other. Therefore, one might expect the data from these U-Pods to be very similar.
15 Indeed, D0 and DE have similar data cloud shapes in Fig. 7. However, the data from the U-Pod at D3 looks to be rather different. This could indicate a localized source is affecting the ozone concentrations at that site. Perhaps a local emission of NO was scavenging ozone at Industrial Zone 1 as a result of industrial operations. Alternatively, this difference could be caused by unique meteorological conditions at this site. The lower ozone values of D3 compared to D7, also appears more pronounced on weekdays (Fig. A2).

20 U-Pod DA was the farthest away from the other monitors, while DC and DB were closer together. However, it was DA and DB that have a similar spread of data around the 1:1 line, and a similar curve of data points below the main data cloud. In other words, DA and DB were more similar than DC and DB even though these two U-Pods were closer together. A possible explanation for this may be proximity to a road. DC is closest to the major roadway, highway 91.

25 Temporal variation in ozone values can be visually examined in more detail by singling out certain hours of data, compared to the full set. Figures 8 and 9 demonstrate this idea.

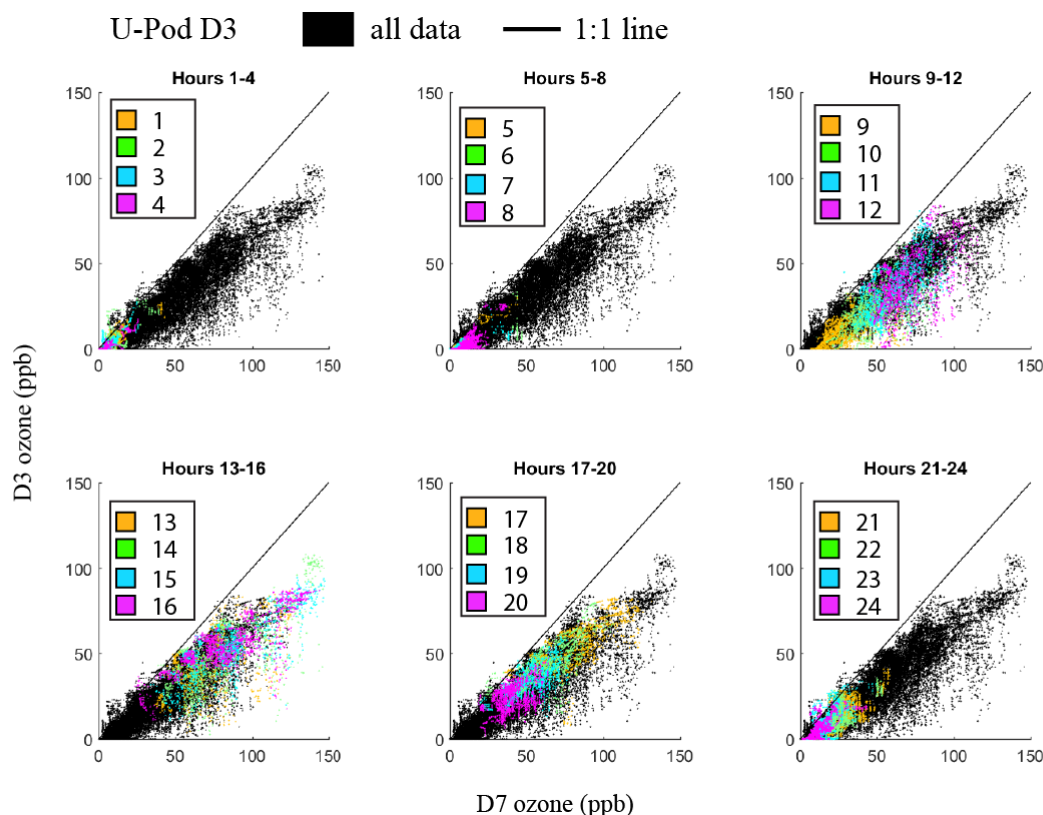


Figure 8. This plot is for U-Pod D3, at Industrial Zone 1. Each scatterplot is four hours of the day, with the black data representing the complete deployment dataset (all hours) and data points recorded within each hour bin are marked by the colors and times in the legend.

5

Figure 8 shows the comparison of D3 with D7 by time of day. Beginning in hour 9:00 and extending through hour 12:00, there were general increases in the ozone concentrations recorded, and the points start to spread out, demonstrating significant spatial variations that are temporally relevant. From hours 13:00 to 16:00, there was less of a trend in terms of generally increasing or decreasing, and values cover a large range of ozone. From 17:00 – 20:00, we observed a reversal of the trend in the 9:00 – 12:00 hour block as ozone starts to decrease again and becomes more densely clustered. The reversed color trend from left to right in these two subplots is very clear. Lastly, for the remaining hours of the day, the measurements become very dense and values decrease again, completing a daily cycle.

10

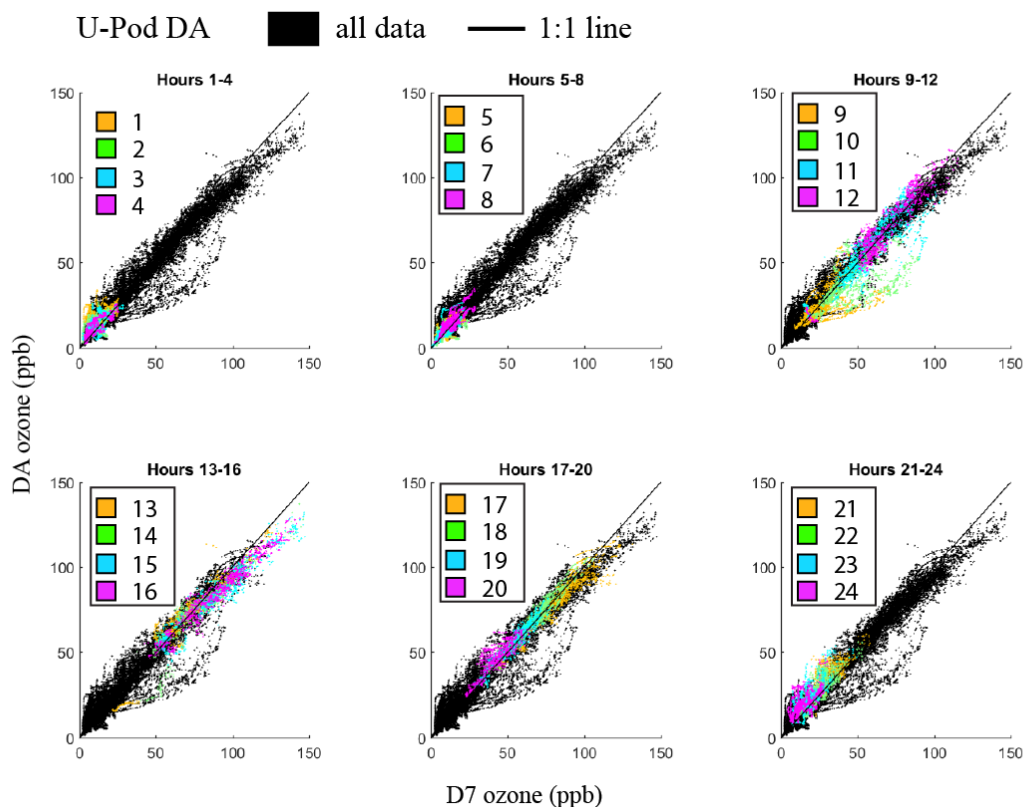


Figure 9. This plot is for U-Pod DA, located at Commercial Zone 1. Each scatterplot is four hours of the day, with the black data representing the complete deployment dataset (all hours) and data points recorded within each hour bin are marked by the colors and times in the legend.

5

Figure 9 shows the relationship between U-Pod DA and U-Pod D7; there were some obvious differences between U-Pods D3 and DA. For U-Pod DA, these plots show concentrations relative to D7 remain much more highly clustered than in the same hours for U-Pod D3. There was far less spread, which indicates that ozone from U-Pods D7 and DA were more similar than D7 and D3. Also of interest is the strange claw shape on the underside of the black data cloud. The analysis in Fig. 9 was conducted for all pods, but not all are shown here. It appears that many of these points occur mostly in hours 9:00 through 11:00 for all affected U-Pods. So, what is happening at the DA site between 9:00 and 11:00 that was not happening between 7:00 and 9:00 or later in the day? The demonstration of variability within this two hour period may be a result of localized ozone precursor emissions such as NO_x or reactive organic gases (ROGs) which happen to correlate with morning rush hour. This claw-shape occurs at the D0, DB, and DE sites as well, all of which are closest to Van Buren Blvd. Also, the data within this claw shape appear to happen more often on the weekend than on weekdays (Fig. A2). We do not have sufficient data on NO_x concentrations or high-resolution traffic information to draw specific conclusions about how these may be affecting ozone at different sites. This could be an area for future research.

15

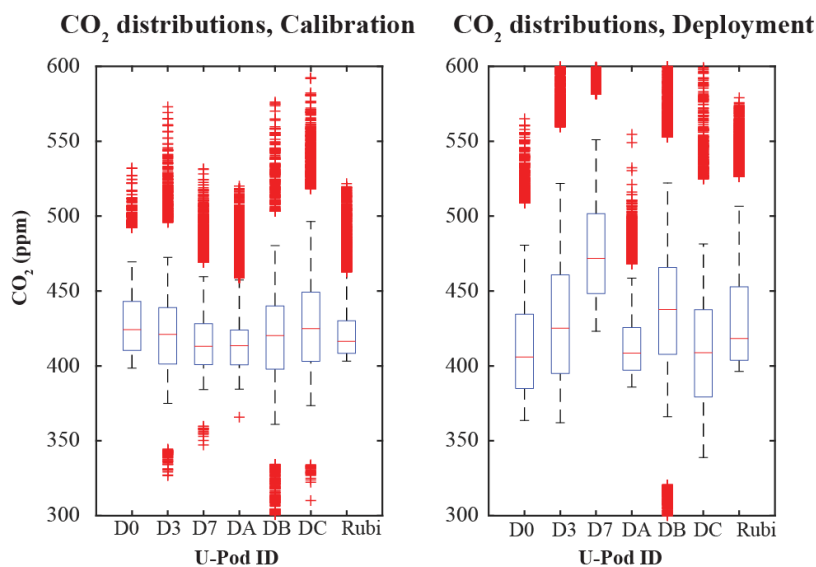


3.4.2 Carbon Dioxide

Carbon Dioxide was continuously measured at the same temporal resolution as ozone in the U-Pods over the same time period. CO₂ data from U-Pods D0, D3, D7, DA, DB, and DC were used for this section of the analysis, based on completeness, reasonable baselines, and no obvious trends through time which may signal sensor drift.

5

To explore the ability to detect spatial differences in carbon dioxide, we compared the distributions of measurements between the calibration time period and that of the deployment, as shown in Fig. 10.



10

Figure 10. Distributions of carbon dioxide measurements from the (a) calibration and (b) deployment time periods. Whiskers indicate the 5th and 95th percentile, with + marks falling outside of this range. The box boundaries span the 25th to 75th percentiles. “Rubi” is shorthand for carbon dioxide concentrations measured at Rubidoux AQMS with a LI-840a gas analyzer, which is not managed by SCAQMD.

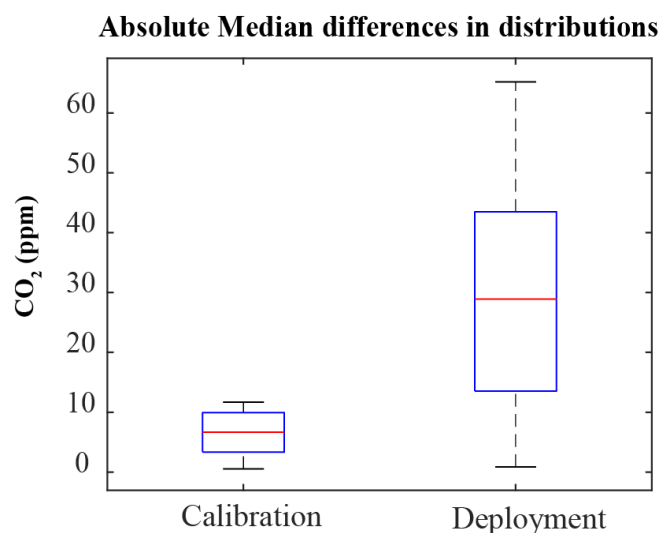
15

The medians of each pod carbon dioxide distributions vary from 413 – 425 ppm during the calibration and 406 – 472 ppm during the deployment. Several differences in the distributions are visible between the two time periods. U-Pod D7 observed higher carbon dioxide measurements during the spatial deployment as compared to the collocated calibration whereas some U-Pods, like DA, have more similar measurements across the two. To more clearly see the variability of measurements between the two time periods, absolute differences between U-Pods were examined. Figure 11 shows the median absolute differences for every possible pair of U-Pods in two groups, calibration and deployment. The differences between U-Pods when they are

20



collocated were small compared to difference between U-Pods when they are dispersed. Some of these differences are greater than the uncertainty of 15 ppm, demonstrating spatial variability.



5 **Figure 11. absolute differences of distribution medians over the two time periods: calibration and deployment.**

We further examined the spatial CO₂ differences by comparing hourly CO₂ concentrations at each site, see Fig. 12. Carbon dioxide values are affected by anthropogenic, biogenic, and atmospheric phenomena. The similar peaks and troughs in the trends likely corresponded to changes in height of the boundary layer. A shorter boundary layer during nighttime would concentrate pollutants, while a larger boundary layer would dilute them. Most of the minimum median CO₂ concentrations occur around 16:00, which is consistent with another LA carbon dioxide study (Newman et al., 2013).

10

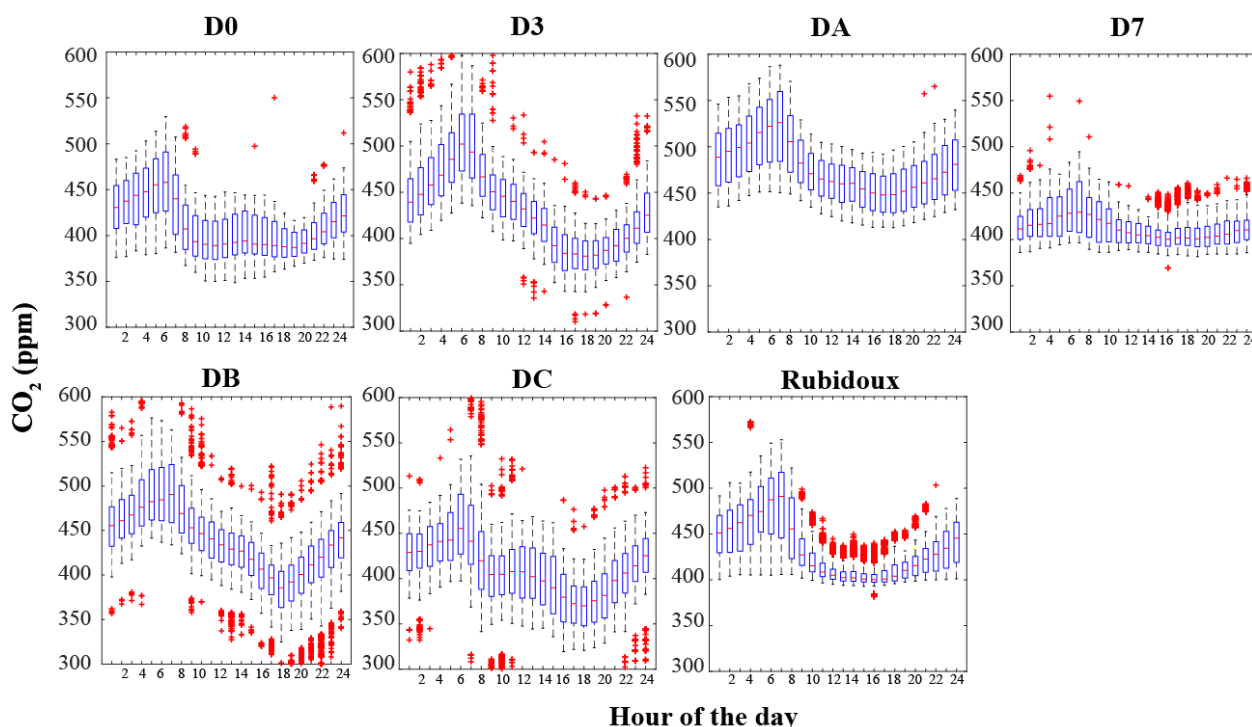


Figure 12. Hourly distributions of carbon dioxide over the deployment period, including the reference data.

The distributions shown in Figure 12 were similar in several ways. Between 6:00 and 8:00, carbon dioxide concentrations were at their peak, and the lowest values occur between 16:00 and 19:00. However, some U-Pods had different distributions in terms of range of data and apparently shifted baselines. The carbon dioxide at Rubidoux station almost never recorded data below 400 ppm, while all the U-Pods except DA do. Also, there appear to be two types of shapes of hourly data. D0, DA, D7, and Rubidoux belong to one group, in which the minimum and maximum medians are closer together. D3, DB, and DC all have minimum values that are much lower than the early morning peaks. The pods that have more similar trends are not closer together than the others. Differences in the trends between hours might be related to traffic counts, or amount of vegetation. Further investigation is warranted.

4 Conclusions

In the region of Riverside, CA, we were able to observe spatial and temporal variability of ozone across an area of roughly 300 km². Field validation of sensor O₃ and CO₂ measurements to minute resolution reference observations resulted in R² and RMSE of 0.95 – 0.97 and 4.4 – 7.2 ppbv for ozone and 0.79 and 15 ppmv for carbon dioxide, respectively. The Thermo Scientific Model 49i Ozone Analyzer that SCAQMD uses for FRM has an acceptable measurement noise of 5% of the precision gas input, or around 5 ppb for ozone. The measurements from the MiCS 2611 O₃ sensor should not be thought of as a way to



replace regulatory air quality monitoring stations, but rather supplement that information. Technological difficulties of obtaining sensor data through environmental extremes, increased sensor variability with high ozone values, electrical issues and data retrieval are all issues encountered when using a U-Pod sensor network. Although the sensors themselves are low-cost, the data retrieval, validation and analysis are not. This work takes more time to perform, and requires more people than more expensive, but user-friendly regulatory procedures and equipment. Future projects may involve very large numbers of sensors, therefore time expenditure for this network method needs to be reduced.

For ozone analysis, the data show the highest amount of variability between U-Pods based on the R-squared values of all their possible pairs to occur between 21:00 and 3:00, as well as at 9:00. U-Pods are more correlated around 5:00, and the period between 11:00 and 19:00. Based on the median absolute differences between all possible pod pairs, the U-Pods are most similar at 6:00, and peaks in differences (least similar) occur at 10:00 and 15:00 – 16:00.

For CO₂ trends, it appears that this S200/300 CO₂ sensor from ELT Corp. auto-calibrating feature caused issues for characterizing the sensor signal over time leading to issues applying calibration models to raw data. U-Pod CO₂ data from the calibration period do not have as high of correlations with each other as those from the ozone data. However, it is still possible to see differences greater than their uncertainty between U-Pods during the deployment, indicating measurable heterogeneity across the study area.

For future research, it is important to collocate the sensors frequently in order to adjust the linear regression coefficients, and therefore provide a better estimate of values throughout the whole deployment. Another area to examine for sensor quantification could be different mathematical approaches to the linear regression. Since higher values of ozone are of the greatest interest to regulators and the public from a human health standpoint, and the sensor variability increases at those higher values, perhaps the regression could be fit differently to suit those needs. An example could be to fit a piecewise function, to better capture the low-ozone and high-ozone regimes separately, or a non-linear model.

Additionally, including measurements of other compounds in the study could help to explain causes for spatial and temporal variability in both ozone and carbon dioxide. For example, including information on nitrogen oxides could help inform the effects on traffic on these compounds, while land use data could reveal the effect of vegetation or industrial operations on measurements.

30 **Code and Data availability**

The final, filtered dataset and the codes used to make the plots in this manuscript are available on Mendeley at DOI: 10.17632/j36zwxxy8v4.1. All codes used to perform the linear regression are not included. It would require a lot of extra work



from co-authors to guide a third party through their use. Raw data are not included because they cannot be interpreted in concentrations without the regression model codes, and results from raw voltages could be misleading. Reference data provided by SCAQMD did not undergo usual procedures of quality assurance and quality control before they were provided to us. Also, SCAQMD did not operate or maintain the LI-840a gas analyzer that collected the CO₂ reference data.

5

10

15

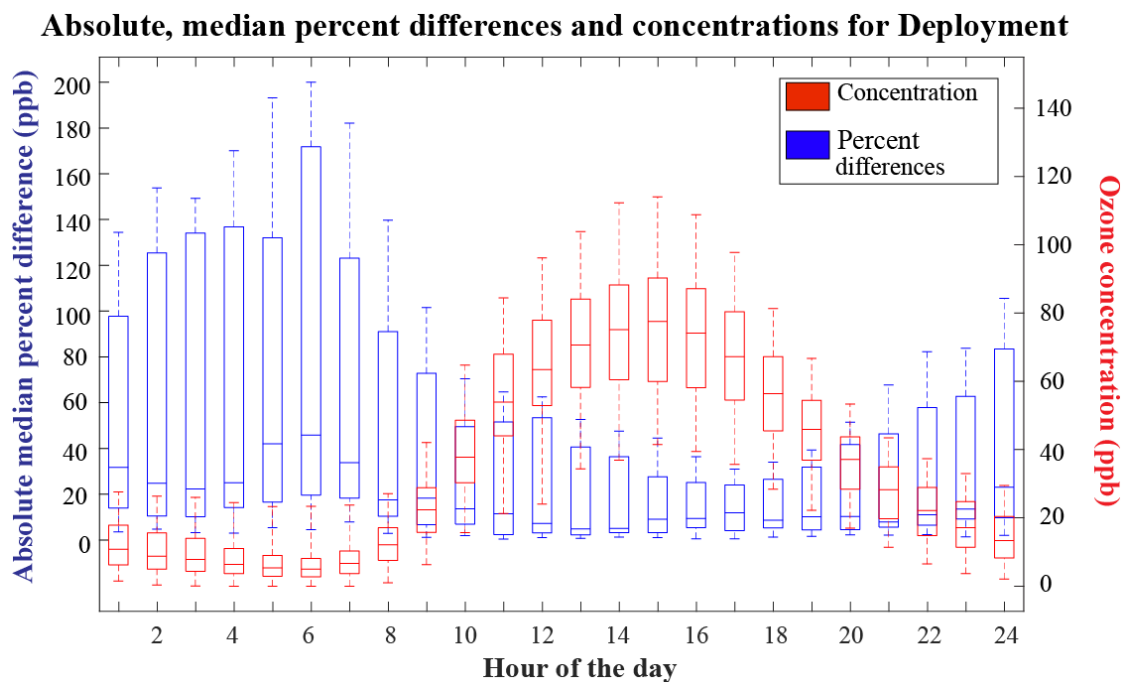
20

25

30



Appendix A



5 **Figure A1.** The right-hand axis shows the distribution of ozone concentrations from all U-Pods for each hour of the day over the deployment. The left-hand axis is the relative percent differences in concentration between all possible pod pairs. Percent difference is used here as the difference in concentration between two U-Pod pairs, normalized by their average. Whiskers indicate the 5th and 95th percentile, values outside of this range are not shown. The box boundaries span the 25th to 75th percentiles.

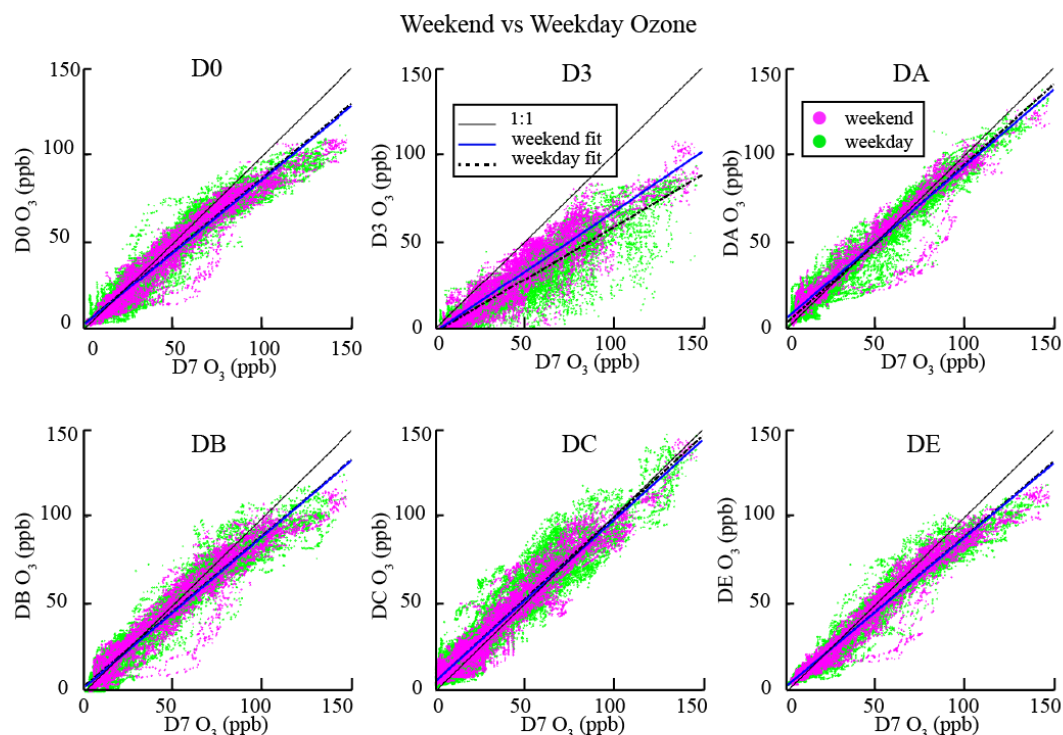


Figure A2. During the deployment period, the magenta data represents data points recorded on the weekend, while green data was recorded during the week. Each subplot is a different U-Pod compared to U-Pod D7 ozone.

Author Contributions

- 5 K. Sadighi helped conduct the field experiment and analyze deployment data, and prepared the manuscript with contribution from all authors. E. Coffey was the lead field scientist, performed the calibrations, and conducted the literature review. A. Polidori and B. Feenstra facilitated collaboration between the Hannigan group and the South Coast Air Quality Management District and provided useful information on air quality conditions in Riverside County. Q. Lv, D. K. Henze, and M. Hannigan provided guidance and academic support for the project.

10 Competing Interests

The authors declare that they have no conflict of interest.



Acknowledgements

This material is based upon work supported by the National Science Foundation under grant no. 1442971. Thank you to members of the Hannigan group for your help: Ashley Collier, Ricardo Piedrahita, and Joanna Casey, and Drew Meyers for your support. Also, thanks to our field tech, Brandon Wong.

5

References

- 2015 Traffic Volumes. Caltrans. Available from: <http://www.dot.ca.gov/trafficops/census/volumes2015/> (Accessed 3 Feb. 2016), n.d.
- Annual Monitoring Network Report for Twenty-three Districts in California. Rep. California Air Resources Board, July 2013. Available from: <https://www.arb.ca.gov/aqd/amnr/amnr2013.pdf>, (Accessed 1 Feb. 2017).
- Bogue, R.: Recent developments in MEMS sensors: a review of applications, markets and technologies, *Sensor Review*, 33(4), 300–304, doi:10.1108/SR-05-2013-678, 2013.
- Bart, M., Williams, D. E., Ainslie, B., McKendry, I., Salmond, J., Grange, S. K., Alavi-Shoshtari, M., Steyn, D. and Henshaw, G. S.: High Density Ozone Monitoring Using Gas Sensitive Semi-Conductor Sensors in the Lower Fraser Valley, British Columbia, *Environ. Sci. Technol.*, 48(7), 3970–3977, doi:10.1021/es404610t, 2014.
- 15 Blanchard, C. L., Tanenbaum, S. and Hidy, G. M.: Spatial and temporal variability of air pollution in Birmingham, Alabama, *Atmospheric Environment*, 89, 382–391, doi:10.1016/j.atmosenv.2014.01.006, 2014.
- Environmental Protection Agency. Ambient Air Quality Surveillance (40 CFR part 58), 2006. Available from : <https://www.ecfr.gov/cgi-bin/retrieveECFR?n=40y6.0.1.1.6>, (Accessed 22 November 2016).
- 20 Environmental Protection Agency. National Ambient Air Quality Standards (40 CFR part 50), 2013. Available from: https://www.ecfr.gov/cgi-bin/text-idx?tpl=/ecfrbrowse/Title40/40cfr50_main_02.tpl, (Accessed 2015).
- Environmental Protection Agency. "Green Book 8-Hour Ozone (2008) Area Information.", 2016. Available from: <https://www.epa.gov/green-book/green-book-8-hour-ozone-2008-area-information>, (Accessed 21 Sept. 2016)
- Gao, H. O.: Day of week effects on diurnal ozone/NO_x cycles and transportation emissions in Southern California, *Transportation Research Part D: Transport and Environment*, 12(4), 292–305, doi:10.1016/j.trd.2007.03.004, 2007.
- 25 Gao, H. O. and Niemeier, D. A.: The impact of rush hour traffic and mix on the ozone weekend effect in southern California, *Transportation Research Part D: Transport and Environment*, 12(2), 83–98, doi:10.1016/j.trd.2006.12.001, 2007.
- Hutyra, L. R., Duren, R., Gurney, K. R., Grimm, N., Kort, E. A., Larson, E. and Shrestha, G.: Urbanization and the carbon cycle: Current capabilities and research outlook from the natural sciences perspective, *Earth's Future*, 2(10), 2014EF000255, doi:10.1002/2014EF000255, 2014.
- 30 Jacob, D. J.: Heterogeneous chemistry and tropospheric ozone, *Atmospheric Environment*, 34(12–14), 2131–2159, doi:10.1016/S1352-2310(99)00462-8, 2000.



- Jiao, W., Hagler, G., Williams, R., Sharpe, R., Brown, R., Garver, D., Judge, R., Caudill, M., Rickard, J., Davis, M., Weinstock, L., Zimmer-Dauphinee, S. and Buckley, K.: Community Air Sensor Network (CAIRSENSE) project: evaluation of low-cost sensor performance in a suburban environment in the southeastern United States, *Atmos. Meas. Tech.*, 9(11), 5281–5292, doi:10.5194/amt-9-5281-2016, 2016.
- 5 Korotcenkov, G.: Metal oxides for solid-state gas sensors: What determines our choice? *Materials Science and Engineering: B*, 139(1), 1–23, doi:10.1016/j.mseb.2007.01.044, 2007.
- Kort, E. A., Angevine, W. M., Duren, R. and Miller, C. E.: Surface observations for monitoring urban fossil fuel CO₂ emissions: Minimum site location requirements for the Los Angeles megacity, *J. Geophys. Res. Atmos.*, 118(3), 1577–1584, doi:10.1002/jgrd.50135, 2013.
- 10 Kumar, P., Morawska, L., Mahtani, C., Basks, G., Neophytou, M., Di Sabatino, S., Bell, M., Norford, L. and Ritter, R.: The rise of low-cost sensing for managing air pollution in cities, *Environment International*, 75, 199–205, doi:10.1016/j.envint.2014.11.019, 2015.
- Lin, C., Gillespie, J., Schuder, M. D., Duberstein, W., Beverland, I. J. and Heal, M. R.: Evaluation and calibration of Aeroqual series 500 portable gas sensors for accurate measurement of ambient ozone and nitrogen dioxide, *Atmospheric Environment*, 100, 111–116, doi:10.1016/j.atmosenv.2014.11.002, 2015.
- 15 Littman, F. E. and Magill, P. L.: Some Unique Aspects of Air Pollution in Los Angeles, *Air Repair*, 3(1), 29–34, doi:10.1080/00966665.1953.10467586, 1953.
- Mead, M. I., Popoola, O. A. M., Stewart, G. B., Landshoff, P., Calleja, M., Hayes, M., Baldovi, J. J., McLeod, M. W., Hodgson, T. F., Dicks, J., Lewis, A., Cohen, J., Baron, R., Saffell, J. R. and Jones, R. L.: The use of electrochemical sensors for monitoring urban air quality in low-cost, high-density networks, *Atmospheric Environment*, 70, 186–203, doi:10.1016/j.atmosenv.2012.11.060, 2013.
- 20 Moltchanov, S., Levy, I., Etzion, Y., Lerner, U., Broday, D. M. and Fishbain, B.: On the feasibility of measuring urban air pollution by wireless distributed sensor networks, *Science of The Total Environment*, 502, 537–547, doi:10.1016/j.scitotenv.2014.09.059, 2015.
- 25 Newman, S., Jeong, S., Fischer, M. L., Xu, X., Haman, C. L., Lefer, B., Alvarez, S., Rappenglueck, B., Kort, E. A., Andrews, A. E., Peischl, J., Gurney, K. R., Miller, C. E. and Yung, Y. L.: Diurnal tracking of anthropogenic CO₂ emissions in the Los Angeles basin megacity during spring 2010, *Atmospheric Chemistry and Physics*, 13(8), 4359–4372, doi:10.5194/acp-13-4359-2013, 2013.
- Piedrahita, R., Xiang, Y., Masson, N., Ortega, J., Collier, A., Jiang, Y., Li, K., Dick, R. P., Lv, Q., Hannigan, M. and Shang, L.: The next generation of low-cost personal air quality sensors for quantitative exposure monitoring, *Atmospheric Measurement Techniques*, 7(10), 3325–3336, doi:10.5194/amt-7-3325-2014, 2014.
- 30 Simon, H., Wells, B., Baker, K. R. and Hubbell, B.: Assessing Temporal and Spatial Patterns of Observed and Predicted Ozone in Multiple Urban Areas, *Environ. Health Perspect.*, 124(9), 1443–1452, doi:10.1289/EHP190, 2016.



South Coast Air Quality Management District (SCAQMD). Air Quality Monitoring Network Plan. Site Plan Rubidoux.

Available from: <http://www.aqmd.gov/docs/default-source/clean-air-plans/air-quality-monitoring-network-plan/aaqmnp-rubidoux.phttp://www.atmos-chem-phys-discuss.net/acp-2016-850/acp-2016-850.pdf.df?sfvrsn=11>, (Accessed 12 Dec. 2015).

- 5 U.S. EPA. 2013 Final Report: Integrated Science Assessment of Ozone and Related Photochemical Oxidants. U.S. Environmental Protection Agency, Washington, DC, EPA/600/R-10/076F, 2013.

Verhulst, K. R., Karion, A., Kim, J., Salameh, P. K., Keeling, R. F., Newman, S., Miller, J., Sloop, C., Pongetti, T., Rao, P., Wong, C., Hopkins, F. M., Yadav, V., Weiss, R. F., Duren, R. and Miller, C. E.: Carbon Dioxide and Methane

- 10 Measurements from the Los Angeles Megacity Carbon Project: 1. Calibration, Urban Enhancements, and Uncertainty Estimates, Atmos. Chem. Phys. Discuss., 2016, 1–61, doi:10.5194/acp-2016-850, 2016.

Williams, D. E., Henshaw, G. S., Bart, M., Laing, G., Wagner, J., Naisbitt, S. and Salmond, J. A.: Validation of low-cost ozone measurement instruments suitable for use in an air-quality monitoring network, Meas. Sci. Technol., 24(6), 065803, doi:10.1088/0957-0233/24/6/065803, 2013.

15

20

25

30



Tables

Table 1: Field calibration results of the Linear 4T model for ozone sensors showing R² and RMSE with the reference monitor data. Two O₃ entries means there are two different sensors in the same U-Pod.

U-Pod ID	D0	D3	D4	D5	D6	D7	D8	DA	DB	DC	DD	DE	DF
R², RMSE	0.98, 3.1	0.98, 3.0	0.98, 2.6	0.99, 2.7	0.98, 3.5	0.98, 2.8	0.98, 3.0	0.97, 3.9	0.98, 2.8	0.99, 2.6	0.99, 1.8	0.97, 3.4	0.98, 3.1
	0.98, 3.2	0.98, 3.0	0.98, 2.7	0.98, 3.0	0.99, 2.4	0.98, 3.0		0.97, 3.9		0.98, 2.7	0.99, 1.8	0.98, 2.9	0.98, 3.0

5

10

15

20

25

30



Table 2. Validation sensitivity results showing mean residuals, median residuals, R^2 and RMSE of sensor measurements against Rubidoux or Mira Loma AQMS observations for O_3 (ppbv) and CO_2 (ppmv). Two-hundred iterations of 10% of randomly chosen data was used for validation statistics. The residuals are U-Pod data – reference monitor data with the same time stamps.

5

U-Pod ID/species	mean residual	median residual	mean R^2	mean RMSE
D7 O_3 Sensor 1	2.4 +/- 0.1	1.2 +/- 0.1	0.965 +/- 0.001	5.6 +/- 0.1
D7 O_3 Sensor 2	2.8 +/- 0.1	1.5 +/- 0.1	0.963 +/- 0.001	5.9 +/- 0.1
D0 O_3 Sensor 1	0.7 +/- 0.1	0.8 +/- 0.1	0.974 +/- 0.001	4.4 +/- 0.1
D0 O_3 Sensor 2	1.1 +/- 0.1	1.0 +/- 0.1	0.971 +/- 0.001	4.9 +/- 0.1
D5 O_3 Sensor 1	5.5 +/- 0.1	5.1 +/- 0.1	0.971 +/- 0.001	5.0 +/- 0.1
D5 O_3 Sensor 2	6.4 +/- 0.1	3.9 +/- 0.1	0.953 +/- 0.001	7.2 +/- 0.1
D7 CO_2	3.0 +/- 0.3	3.0 +/- 0.3	0.789 +/- 0.007	15 +/- 0.2